JOURNAL OF MATERIALS SCIENCE 28 (1993) 2501–2516

Tempering effects on acoustic emission–microstructural relationships in ferritic steels

C. B. SCRUBY, H. N. G. WADLEY*
National NDT Centre, AEA Technology, Harwell Laboratory, Oxfordshire, OXII 0RA UK

A systematic study of the effect of tempering on acoustic emission–microstructure relations has revealed that intermediate tempering treatments of three Fe–3.25 wt % Ni alloys with 0.06, 0.17 and 0.49% carbon lead to a pronounced acoustic activity during subsequent ambient-temperature tensile testing. The maximum emission intensity occurs from samples tempered near 250 °C for 100 min, and increases with carbon content. Mechanical property measurements reveal the emission maximum to be correlated with strengthening, the maximum strengthening (between 250 and 300 °C) coinciding with the maximum emission. The observations can be accounted for by a model which involves the high-speed cooperative motion of groups of dislocations over distances corresponding to the lath packet dimension. The mechanism that induces cooperative dislocation motion is suspected to be a precipitate shearing process, a process that has not been significantly considered for quenched and tempered ferritic steels before. A second, much weaker source of emission has been identified in material subjected to prolonged tempering at 625 °C. The mechanism responsible for this emission is believed to be the rapid multiplication, and high-speed propagation, of groups of dislocations between widely distributed cementite particles. No evidence has been found to support the view that carbide fracture in quenched and tempered steels is a direct source of acoustic emission.

1. Introduction

Ferritic steels constitute an important class of materials where a better understanding of dislocation and crack growth mechanisms is required. Furthermore, for the application of acoustic emission technology to structural monitoring, a knowledge of the source mechanism of detected emissions is essential. In an earlier paper [1], work was presented utilizing acoustic emission to explore the effects of quench rate (from 1000 °C), and therefore of microstructure, upon the micromechanisms of deformation and fracture for a model ferritic steel system in which the carbon content could be adjusted. It was found that in microstructures containing ferrite distributed so that at least one linear dimension of each microstructural unit exceeded ~ 10 μm, the coordinated motion of between 10 and 1000 dislocations at velocities $\sim 10\%$ the speed of sound was able to account for observations of acoustic emission during initial yielding.

Previously reported work on a 0.21% carbon steel similar to one used in the earlier study [2] indicated that cooperative slip phenomena might also occur as a precursor to general yield in martensite tempered between 200 and 400 °C for about 100 min. It has been speculated, on the basis of transmission electron microscopy observations, that these events are linked to the pinning of the quenched-in dislocations by very small carbides. The escape of the dislocations from these precipitates was suggested to be the origin of the detected emission. Alternative explanations are either that the emission is linked with the fracture of lath boundary carbides which exist in a lenticular form in the vicinity of the temperature range of maximum emission [3], or that precipitate shear by dislocations caused local softening, concentrated slip, and thus detectable emission as seen, for instance, in age-hardened aluminium alloys [4]. To begin to resolve these possibilities this paper reports on additional experiments that have been made to investigate more systematically the role of precipitate size, shape, and volume fraction upon the relationship between acoustic emission, deformation micromechisms and microstructure.

2. Experimental procedure

Experiments were performed using samples prepared from three (low sulphur) Fe–3.25% Ni–1% Mn–x% C ingots whose preparation is given elsewhere [1]. Their bulk carbon concentrations (wt %) were 0.06 (steel D), 0.17 (steel E) and 0.49 (steel F). The preparation of samples and their austenitization treatments were identical to those of the samples used previously.

*Present address: Department of Materials Science and Engineering, University of Virginia, Charlottesville, Virginia 22903, USA.

0022–2461

Following austenitization at 1000 °C for 1 h, the samples were oil-quenched and then tempered. Two types of tempering treatment were used. Some samples were isochronally tempered for 100 min at temperatures in the range 50 to 625 °C. The remainder were isothermally tempered at 625 °C for times between 5 and 40 000 min (one month). The shortest tempering times (10 min or less) were sufficient for samples to just reach the furnace temperature. They were included only to give qualitative indications of the early tempering trends. The objective of these treatments was the production of as wide a range of carbide size distributions as possible. The addition of variable carbon concentration (while keeping other compositional variables fixed) provided a method for further changing the carbide volume fraction. Several (four or more) samples of each condition were tested under uniaxial conditions at constant strain rate to reduce scatter. Both mechanical properties and acoustic emission were measured, taking care to ensure identical experimental procedures to those of the earlier study [1] so that quantitative comparisons were possible. Because of the difficulty in characterizing the precipitate distributions of lightly tempered samples in the transmission electron microscope, a selection of medium-carbon samples was examined with small-angle neutron scattering to infer trends in particle size with tempering.

3. Results

3.1. Microstructural characterization

The reader is referred to the earlier study [1] for a microstructural characterization of the oil-quenched state from which all subsequent tempering treatments were derived.

3.1.1. Isochronal tempering

When examined by optical metallography, isochronal tempering for 100 min at ≤ 200 °C was seen to produce imperceptible microstructural changes, i.e. any changes were at the submicrometre level. Tempering at higher temperatures (Fig. 1) produced optically detectable changes. Two effects were observed: a coarsening of precipitates and a transformation of lath martensite to polygonal ferrite subgrains. The intercarbide spacing varied with carbon content and tempering temperature. The widest average intercarbide spacing (1–2 μm) occurred in the low-carbon (0.06% C) alloy tempered at 625 °C. It decreased both with increasing carbon content and decreasing tempering temperature.

To explore the submicrometre microstructural changes, we have used both transmission electron microscopy (TEM) and small-angle neutron scattering (SANS). TEM indicated that tempering at ~ 200 °C caused the precipitation of small (10–100 nm) carbides (Fig. 2). These appeared to have nucleated on the quenched-in dislocations (Fig 2a). They were very difficult to characterize quantitatively, due to the high dislocation density and magnetic aberrations. Other larger precipitates produced during quenching [1] remained in the microstructures of samples tempered below ~ 200 °C (Fig. 2b and c).

Increasing the tempering temperature to > 400 °C resulted in a loss of the small dislocation-nucleated precipitates and the autotempering product, and the appearance of larger precipitates, in some cases nucleated at lath boundaries where they initially assumed a lenticular shape Fig. 2. After tempering at ~ 600 °C, the precipitates assumed a roughly spheroidal shape in all three steels (Fig. 3). No effects of carbon concentration on carbide morphology were seen at the higher tempering temperatures. The main effect of carbon content was to change the volume fraction of carbides.

SANS can be used to characterize precipitation. In contrast to TEM it integrates the scattering from large volumes of material and can provide a clearer view of the coarsening of very small (~ 10 nm) precipitates [5, 6]. Other scattering, e.g. from dislocations, is weak and the contribution from magnetic domains can be reduced by the application of a saturation magnetic field (which aligns the domains). SANS studies of the medium-carbon steel (Fig. 4) indicated extensive scattering to high Q (scattering angle) values in material tempered at ≤ 200 °C. This is indicative of a high density of very small (10–100 nm) scattering centres [5], most probably the dislocation-nucleated precipitates in Fig. 2a. The loss of scattering, especially at high scattering angle, for samples tempered above 200 °C is consistent with a rapid disappearance of the small scattering centres and a decrease in the carbide number density, consistent with a carbide coarsening process [5].

In addition to carbide coarsening, increasing the tempering temperature above 400 °C resulted in the recovery of the quenched-in dislocations and decomposition of the lath martensite to ferrite. This eventually led to an equiaxed ferrite subgrain microstructure, which, after a 600 °C temper, had a subgrain size of ~ 0.5–1.0 μm in the low-carbon steel. The subgrain size decreased with increasing carbon concentration due to subgrain boundary pinning by carbide precipitates.

3.1.2. Isothermal tempering

Optical microscopy was incapable of resolving the effects of tempering for less than 40 min at 625 °C, suggesting that only changes at the submicrometre level occurred. Tempering for ≥ 100 min (Fig. 5) resulted in the nucleation and a gradual coarsening of carbides and recovery recrystallization of the quenched-in dislocation structure, leading eventually to an equiaxed ferrite. The carbide volume fraction increased with carbon content. Since the carbide size was approximately the same in each alloy, the average carbide spacing decreased with carbon concentration. For example, after a 1000 min temper the low-carbon alloy spacing was 2–3 μm, while that of the high-carbon alloy was 1–2 μm.

The ferrite subgrain size of all samples increased slowly with tempering beyond 100 min to reach a value of ~ 4μm after 10 000 min of tempering. TEM studies of samples tempered for less than 40 min were able to resolve microstructural changes analogous to

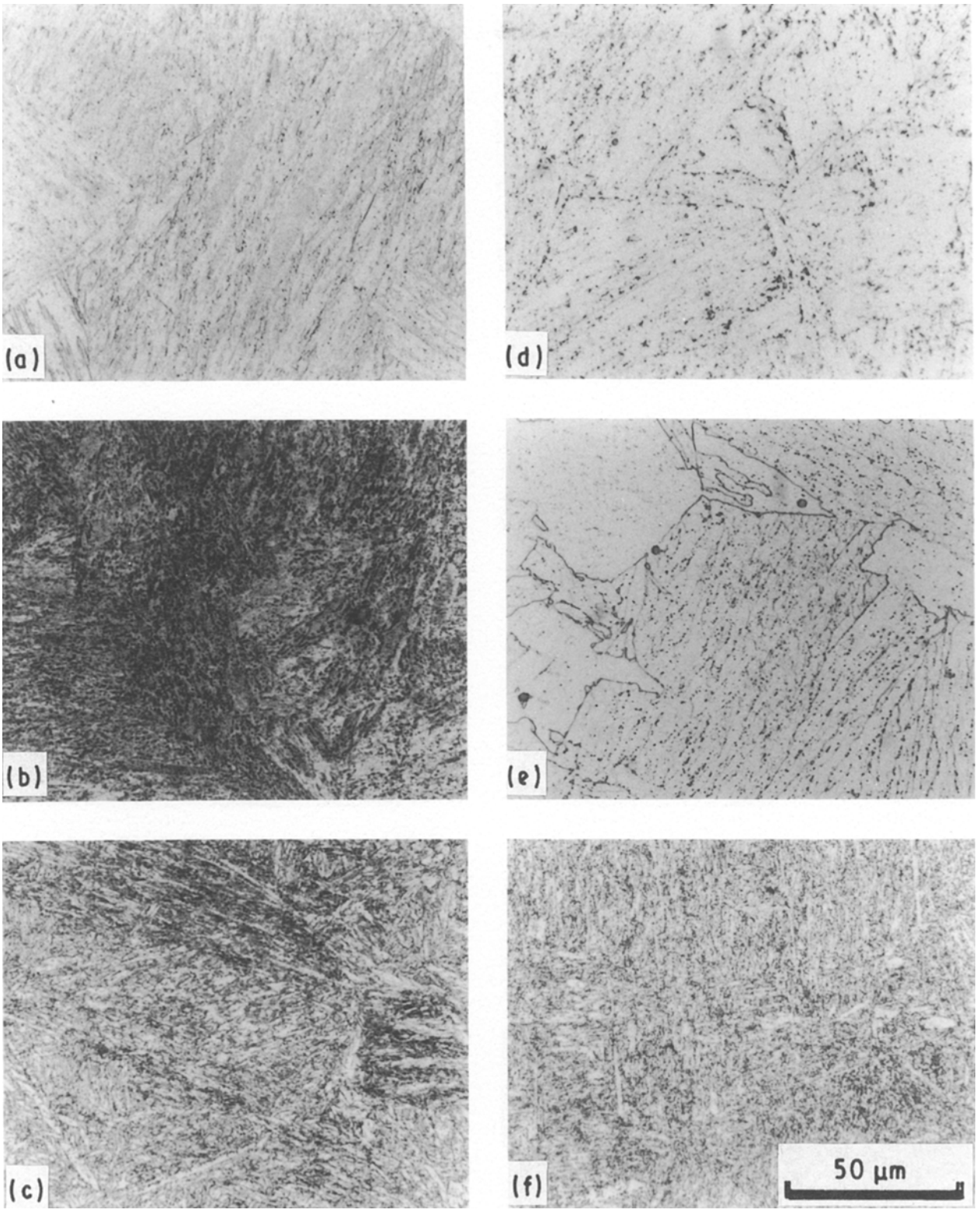

Figure 1 Optical micrographs showing effect of carbon concentration for specimens tempered at (a–c) 403 °C and (d–f) 601 °C (Nital etch): (a, d) 0.06% C; (b, e) 0.17% C; (c, f) 0.49% C.

those of the isochronal tempering treatments. Steels tempered at 625 °C for 5 min had similar microstructures to those tempered in the 300–400 °C range for 100 min. The lath structure was still preserved, dislocation recovery had not begun, and carbides had nucleated both at lath interfaces and on dislocations. Tempering for 10 min was sufficient to cause detectable recovery and the formation of ferrite subgrains, in a manner similar to samples isochronally tempered at ~ 500 °C. Recovery was essentially complete within about 100 min at 625 °C. Extended further tempering at 625 °C resulted in the coarsening of subgrain structure, a typical example of which is shown in Fig. 6. Interestingly, the longest tempers resulted in the ap-

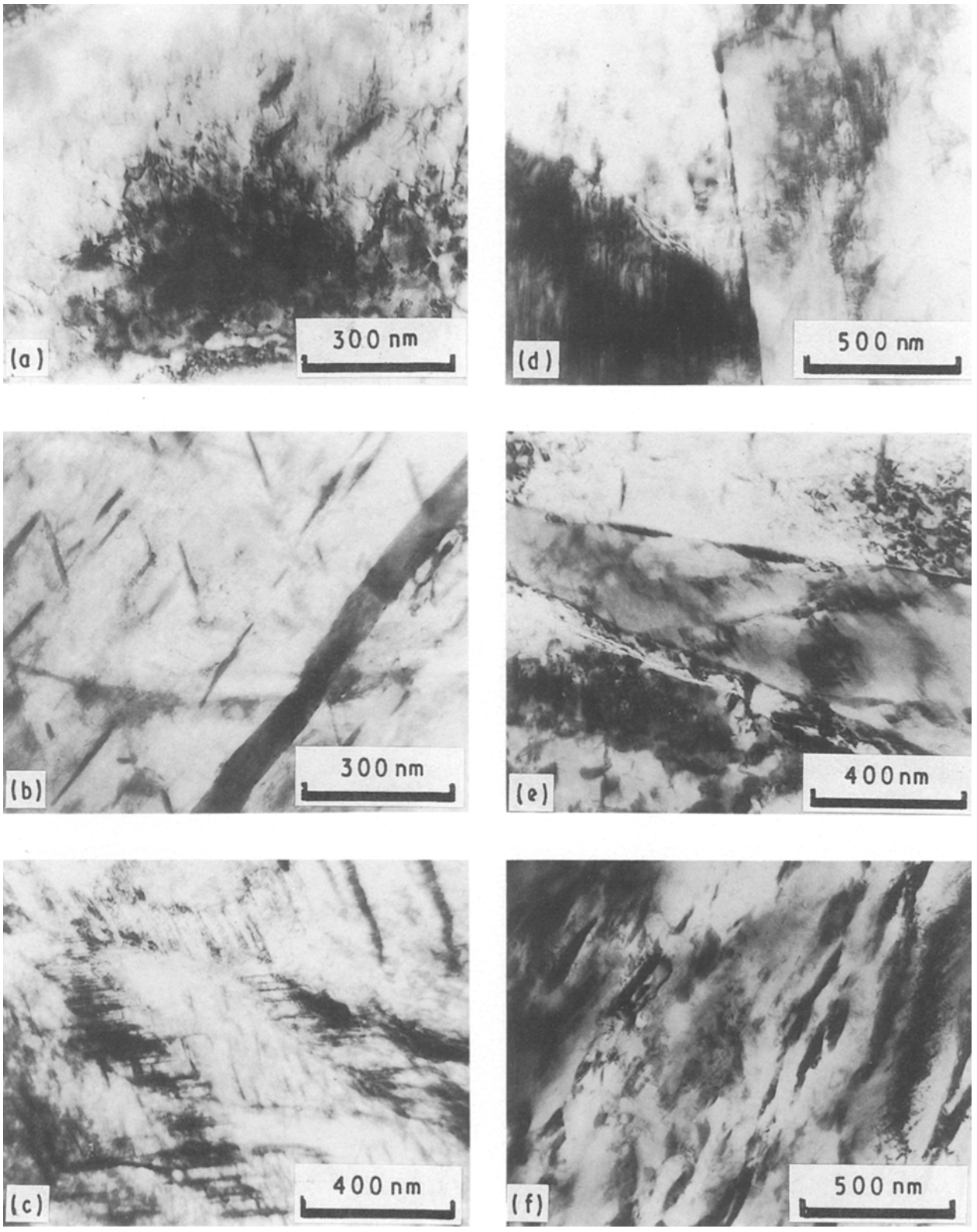

Figure 2 Transmission electron micrographs for specimens isochronally tempered at (a–c) 200 °C and (d–f) 400 °C as a function of carbon concentration: (a, d) 0.06% C; (b, e) 0.17% C; (c, f) 0.49% C.

pearance of small dislocation loops, similar to those seen in radiation-damaged material, presumably due to the agglomeration of quenched-in point defects.

3.2. Acoustic emission

3.2.1. Isochronal tempering

Typical acoustic emission data for isochronally tempered samples are shown in Figs 7 and 8. Following the procedure used before [1], it is useful to examine separately the emission up to maximum nominal stress (region I), and the emission from maximum stress to fracture (region II). The former tends to emphasize plastic deformation sources and the latter microfracture.

It can be seen that in region I, tempering at 250 or 400 °C resulted in the appearance of intense acoustic emission during early yielding. The maximum in

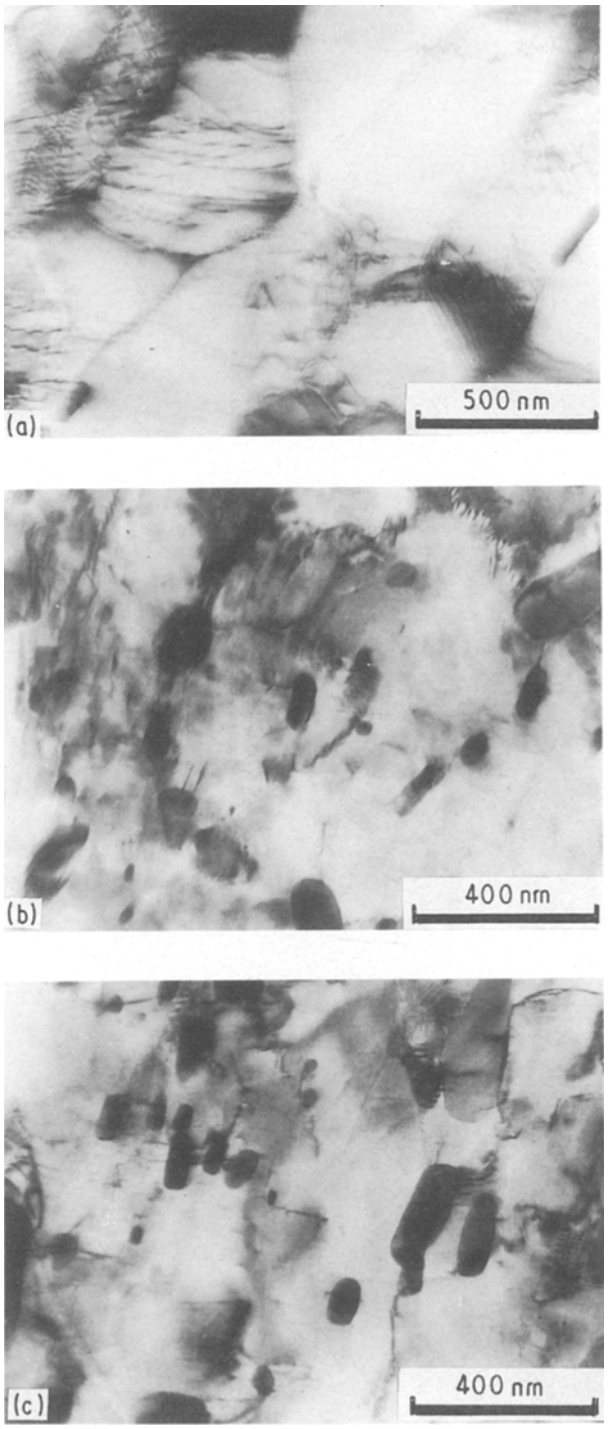

Figure 3 Transmission electron micrographs for specimens isochronally tempered at 600 °C as a function of carbon concentration: (a) 0.06% C, (b) 0.17% C, (c) 0.49% C.

intensity occurred just prior to general yield. When observed on an oscilloscope, the emission was composed of numerous individually weak overlapping signals. The emission rate was so high that sample reverberations (of ~3 ms duration) were unable to decay between events. Tempering above ~400 °C resulted in less emission during yield with almost no emission detectable after tempering at ~600 °C. This behaviour did not seem to be particularly strongly affected by the carbon concentration: only a small increase with increasing carbon content occurred.

The majority of isochronally tempered samples generated little or no acoustic emission in region II. The

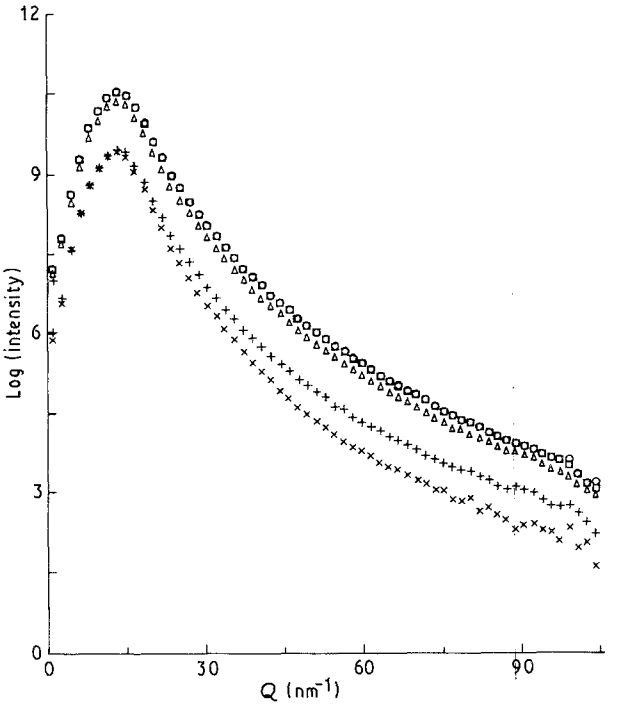

Figure 4 Small-angle neutron scattering intensity versus scattering vector Q for isochronally tempered samples of steel E. Loss of intensity at high Q is indicative of loss of small scattering sites. (○) 95 °C, (□) 148 °C, (△) 198 °C, (+) 283 °C, (×) 403 °C.

exception was the high-carbon steel (steel F) which behaved in a brittle manner (with no region I) when lightly tempered (Fig. 7c). The emission in region II of this sample consisted of discrete signals, relatively few in number, but of individually high energy.

The total acoustic emission energy (the time integral of the acoustic power shown in Figs 7 and 8) was found for each region and is tabulated in Tables I and II, and total acoustic emission energy (regions I and II) has been plotted as function of isochronal tempering temperature in Fig. 9. For the three steels it is observed that:

(i) A sudden increase in emission occurs as the tempering temperature approaches 200–250 °C. (This trend is partially obscured for the high-carbon steel by premature brittle fracture of quenched and lightly tempered states.)

(ii) The maximum acoustic emission arises from samples tempered at between 250 and 300 °C.

(iii) Tempering from 300 to 600 °C results in the gradual disappearance of acoustic emission.

(iv) All three steels show similar tempering trends, although as already noted the behaviour of steel F is truncated at low tempering temperatures by premature brittle fracture.

3.2.2. Isothermal tempering

Typical acoustic emission data for isothermally tempered samples are shown in Fig. 10. Two extreme types of emission behaviour were observed. Samples tempered at 625 °C for 5–10 min generated intense acoustic emission similar in character to that of samples isochronally tempered between 200 and 300 °C.

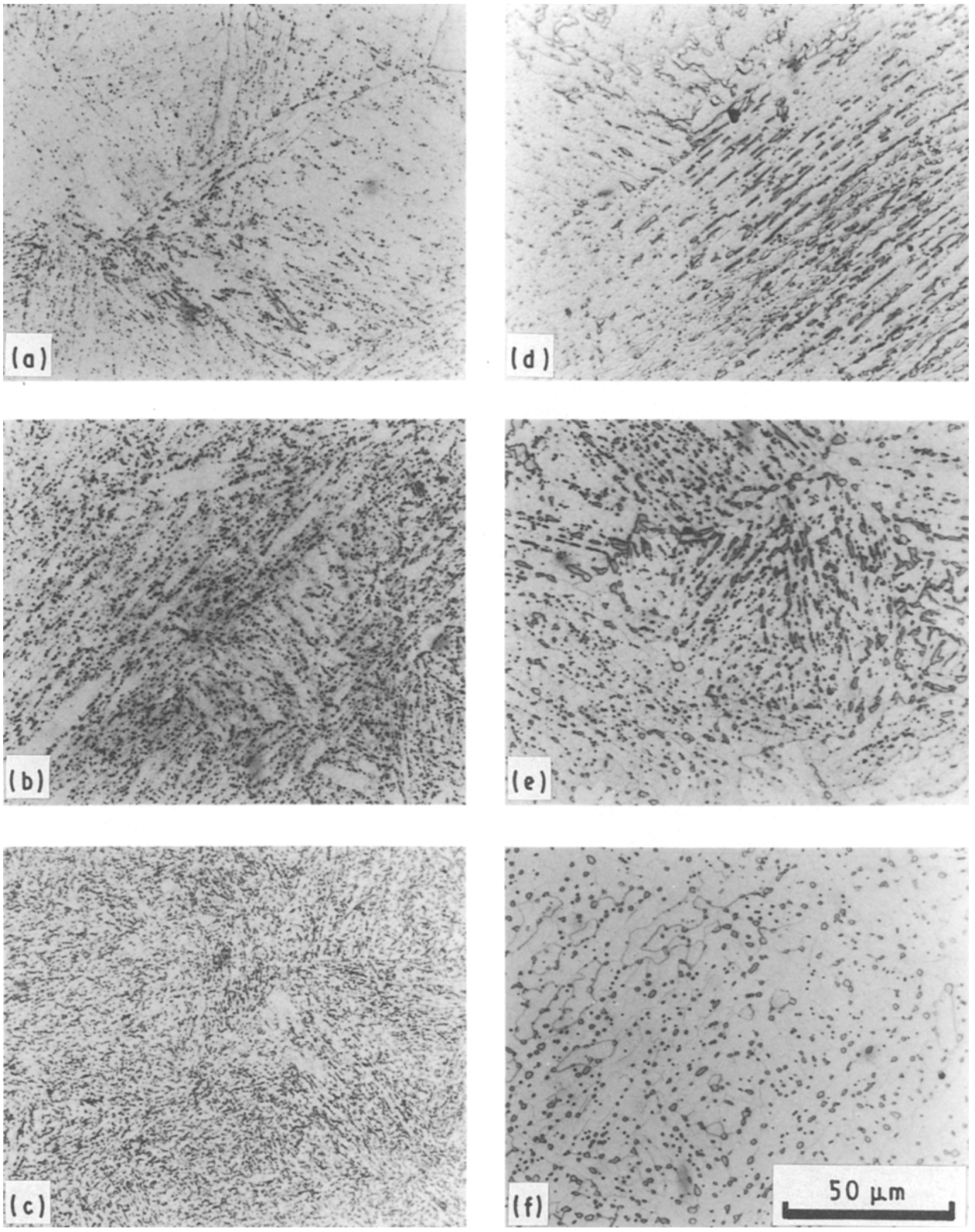

Figure 5 Optical micrographs showing effect of carbon concentration for specimens tempered at 625 °C for (a–c) 1000 min and (d–f) 40 000 min (Nital etch): (a, d) 0.06% C; (b, e) 0.17% C; (c, f) 0.49% C.

This emission seemed not greatly affected by carbon content and was absent if the tempering was extended to 100 min or beyond. Extended tempering (> 1000 min) resulted in Luders band deformation and the appearance of numerous, individually weak emissions that persisted only for the period of band nucleation and propagation (i.e. the flat region of the stress–strain curve). This emission was more pronounced in the higher-carbon steels. It slowly increased in intensity with increasing tempering time.

Data for the acoustic emission energy detected during region I of the stress–strain curve are summarized in Table III, and Fig. 11.

Acoustic emission during region II of all isothermally tempered samples was usually confined to a single emission during final fracture. The energy of this

decreased with tempering time, changing from 0.50, 0.64 and 0.97 mJ to 0.25, 0.38 and 0.46 mJ for steels D, E, and F, respectively, upon tempering.

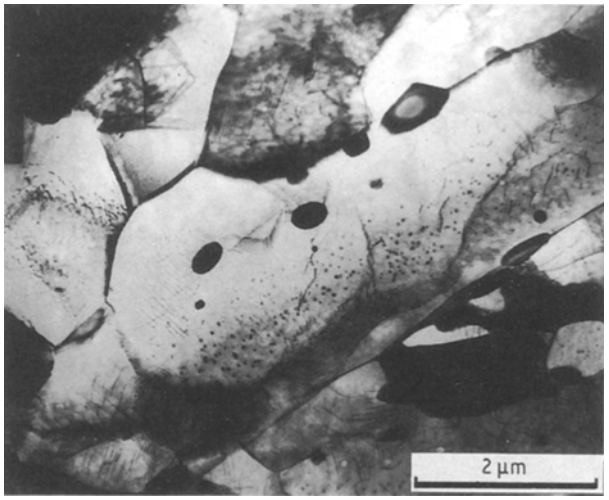

Figure 6 0.17% carbon steel isothermally tempered for 10000 min at 625 °C.

3.3. Mechanical properties

3.3.1. Isochronal tempering

Digitally recorded load–displacement records for each heat-treatment were analysed to obtain various parameters representative of the stress–strain behaviour. These data are shown in Table IV.

It is seen that the strength of any tempered state increases with carbon concentration. Tempering for 100 min at or below 283 °C causes an increase in 0.1% and 0.2% proof stress ($\sigma_{0.1}$ and $\sigma_{0.2}$) (Fig. 12), and in ultimate tensile stress σ_{UTS}. Above 283 °C, the strength began to decrease, the rate of this increasing with increasing carbon content. It is interesting to note that in all three steels, the acoustic emission energy maximum occurred close to the tempering temperature for maximum strength.

The mechanical property measurements indicate that the strain to σ_{UTS} (the maximum uniform strain a sample could support before the onset of localized necking) also depended upon tempering temperature, falling to a minimum of 2–3% after tempering between 250 and 300 °C (slightly higher for steel F). Again, we note that the tempering that resulted in a

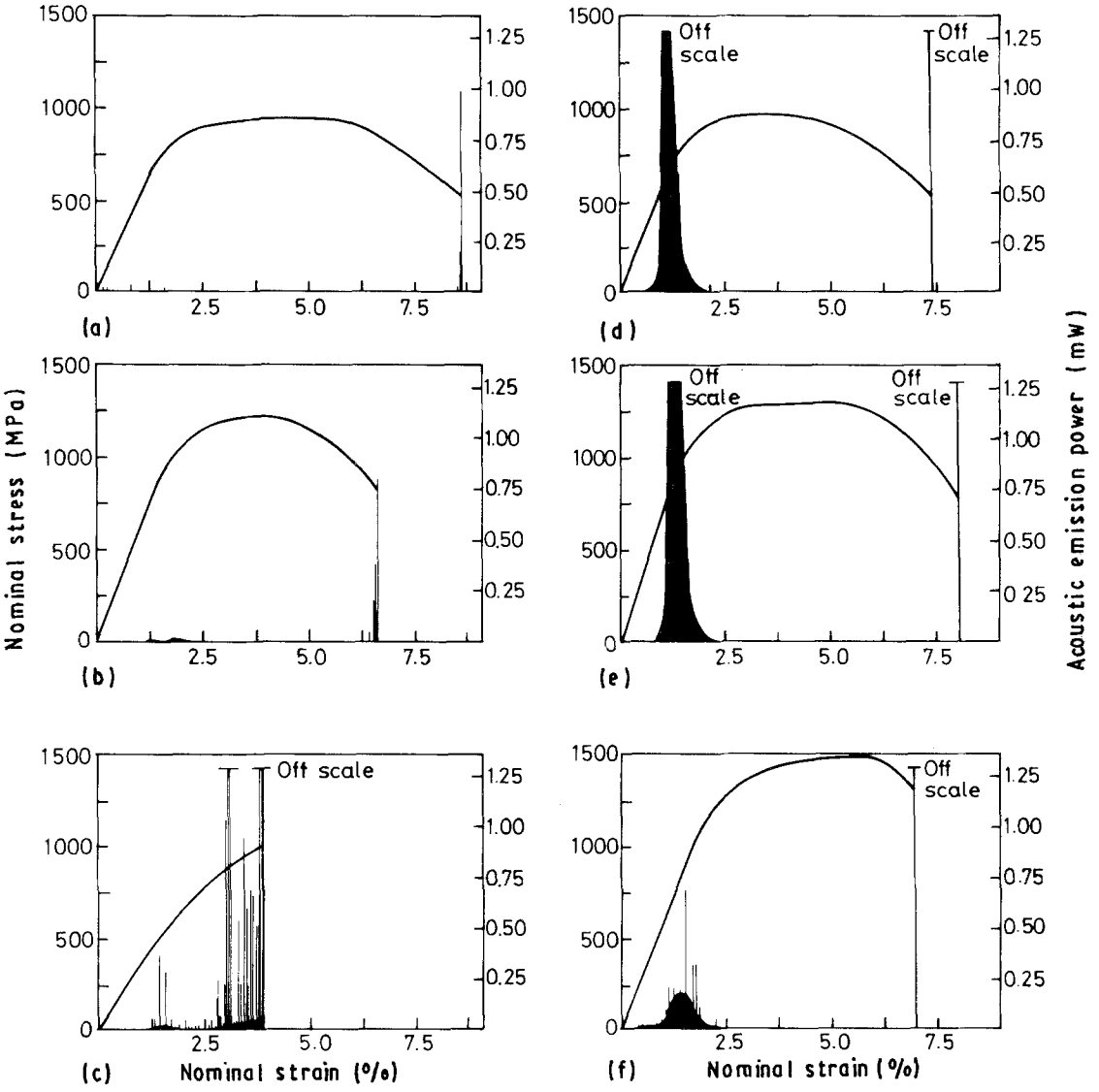

Figure 7 Acoustic emission and stress as functions of strain for specimens isochronally tempered at (a–c) 95 °C and (d–f) 250 °C: (a, d) 0.06% C; (b, e) 0.17% C; (c, f) 0.49% C.

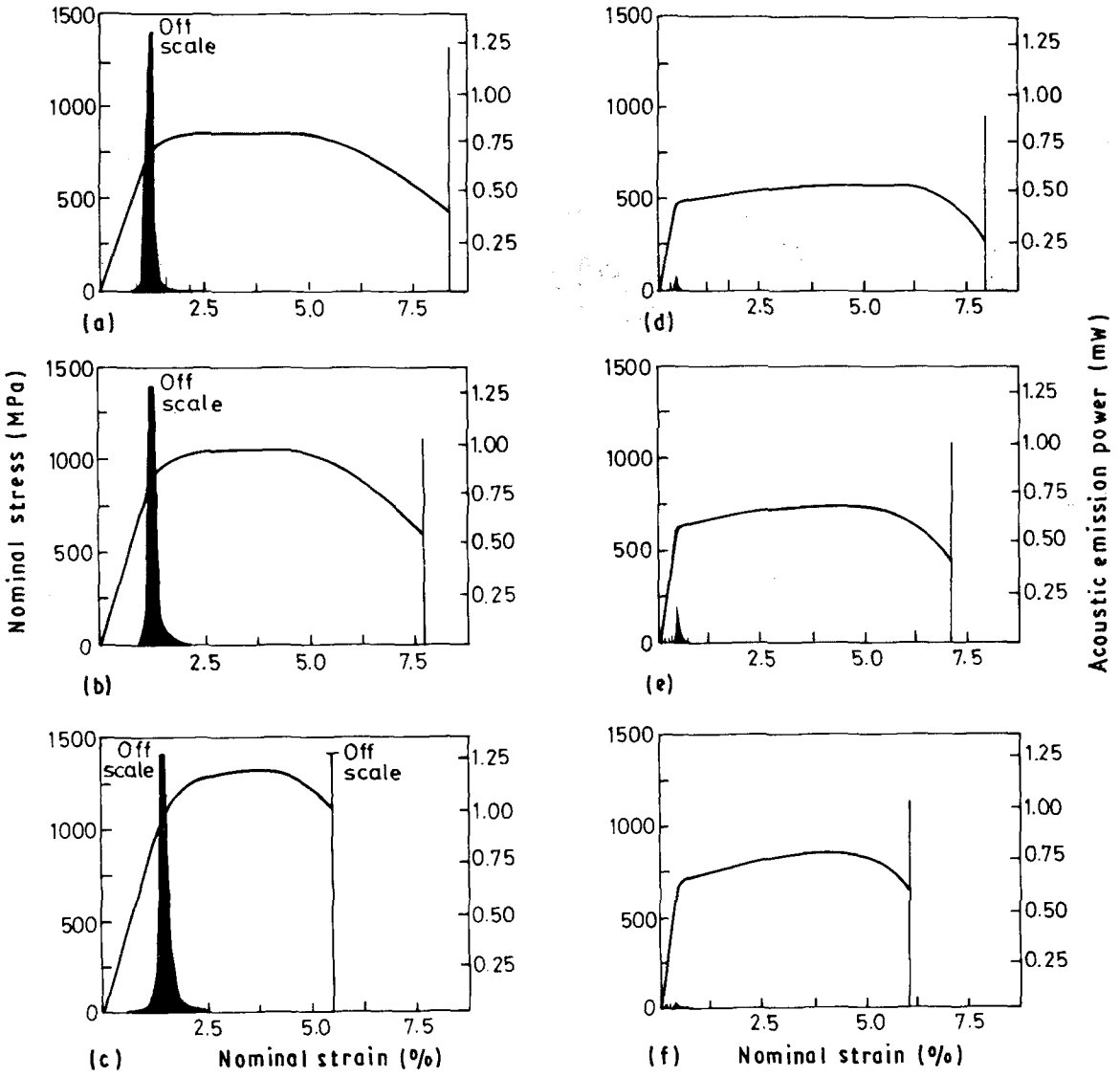

Figure 8 Acoustic emission and stress as functions of strain for specimens isochronally tempered at (a–c) 400 °C and (d–f) 600 °C: (a, d) 0.06% C; (b, e) 0.17% C; (c, f) 0.49% C.

TABLE I Acoustic emission generated by plastic deformation (region I) during isochronal tempering

Heat treatment	Acoustic emission (mJ)		
	Steel D	Steel E	Steel F
Oil quench	1.35	0.03	[a]
Oil quench + 50 °C, 100 min	0.09	0.19	[a]
Oil quench + 95 °C, 100 min	0.26	0.45	[a]
Oil quench + 143 °C, 100 min	0.90	2.93	[a]
Oil quench + 198 °C, 100 min	6.80	18.36	6.49
Oil quench + 250 °C, 100 min	23.10	28.93	8.48
Oil quench + 290 °C, 100 min	22.78	18.64	33.25
Oil quench + 403 °C, 100 min	11.85	10.31	14.42
Oil quench + 502 °C, 100 min	1.94	1.11	3.61
Oil quench + 601 °C, 100 min	0.54	2.01	0.94

[a] Indicates fracture before post maximum stress. Acoustic emission attributed to region II.

TABLE II. Acoustic emission energy generated by fracture (region II) during isochronal tempering

Heat treatment	Acoustic emission (mJ)		
	Steel D	Steel E	Steel F
Oil quench	0.5	0.69	6.45
Oil quench + 50 °C	0.67	0.90	7.42
Oil quench + 95 °C	0.59	0.67	7.50
Oil quench + 143 °C	0.61	0.70	7.85
Oil quench + 198 °C	0.45	0.70	2.88
Oil quench + 250 °C	0.53	0.66	1.64
Oil quench + 290 °C	0.52	0.56	1.33
Oil quench + 403 °C	0.39	0.53	0.74
Oil quench + 502 °C	0.56	0.58	0.57
Oil quench + 601 °C	0.38	0.40	0.57

minimum strain to σ_{UTS} corresponded to that which resulted in both maximum emission and strength.

The effect of tempering temperature upon the work-hardening rate at a plastic strain of 1% (close to the strain at which maximum acoustic emission was observed) is shown in Fig. 13. The low- and medium-carbon steels had lower work-hardening rates than the high-carbon steels for tempering temperatures ≤ 283 °C, reflecting the higher quenched-in dislocation density. Above 283 °C all three steels behaved

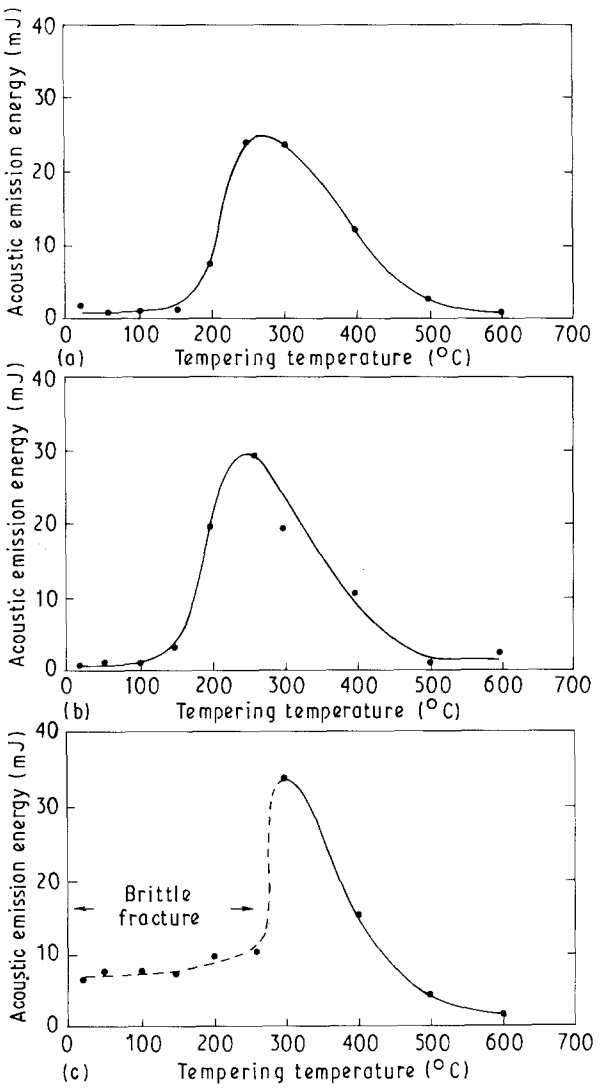

Figure 9 Dependence of total emission energy recorded upon isochronal tempering temperature as function of carbon concentration: (a) 0.06% C, (b) 0.17% C, (c) 0.49% C.

similarly, with a decrease of ~ 50% in work-hardening rate when the tempering temperature was increased from 280 to 600 °C.

3.3.2. Isothermal tempering

Mechanical properties data for isothermally tempered samples are shown in Table V. Short tempering treatments increase the strength of all three alloys, but thereafter the proof stresses and ultimate tensile stresses decrease linearly (composed with quenched data published earlier [1]) with log(time), (Fig. 14). While the strain to σ_{UTS} monotonically increases with tempering time in all three alloys, the non-uniform strain (difference between plastic strain to fracture and plastic strain to σ_{UTS}) decreases after prolonged tempering of the medium- and high-carbon steels. This indicates a decreased resistance to void nucleation, growth and coalescence in these samples.

4. Discussion

The influence of heat treatment and carbon content upon the acoustic emission detected during deformation of these quenched and tempered steels can be conveniently summarized in map form as shown in Fig. 15. Here, the influence of tempering temperature and time have been combined by the use of a Holloman–Jaffe parameter $p = T(k + \log t)/1000$ where T is the absolute tempering temperature, t is the tempering time (min) and k is a constant (~ 20 for alloy steels).

Omitted from the map are the data for samples isothermally tempered for short periods (because of uncertainty regarding the true temperature/time treatment of these samples). Their emission is assumed to arise from the same mechanisms responsible for the high-temperature tail ($p = 12$) of the (isochronal) tempering acoustic emission peak.

The tempering of quenched low-alloy steels clearly has a similar very marked effect upon the acoustic emission detected from deformation in all three steels. The dominant effect is the development of a pronounced isochronal acoustic emission peak centred at ~ 300 °C. A much weaker trend is the gradual reappearance of acoustic emission after prolonged tempering at 625 °C.

To what can we attribute these two effects? In both cases the detected acoustic emission is generated during initial yielding of the samples. Work published elsewhere shows that the effects are not associated with inclusion fracture/decohesion [7, 8]. It is thus reasonable to assume that the effects arise from the motion of dislocations and their interactions with the microstructure. Such dislocation interactions have not previously been well characterized in low-alloy steels, and the acoustic emission measurements give useful insights into dislocation mechanisms in this important class of materials.

TABLE III Acoustic emission generated by plastic deformation (region 1) during isothermal tempering

Heat treatment		Acoustic emission (mJ)		
		Steel D	Steel E	Steel F
Oil quench		1.35	0.03	*
Oil quench + 625 °C,	5 min	23.33	14.72	5.78
	10 min	7.97	1.39	6.62
	40 min	2.32	1.10	2.92
	100 min	1.04	1.00	0.42
	400 min	1.07	1.22	0.38
	1000 min	0.42	0.93	0.32
	4000 min	0.17	1.10	0.38
	10000 min	0.30	1.21	Not measured
	40000 min	0.01	0.98	2.60

4.1. Microstructural changes

The microstructure of the quenched samples of all three steels consists of martensitic laths containing a high density of dislocations. Steels D and E contained isolated regions of carbide precipitation [1] while steel F contained very fine (possible ε carbide) precipitates and internal twins. We believe that the coarse carbides

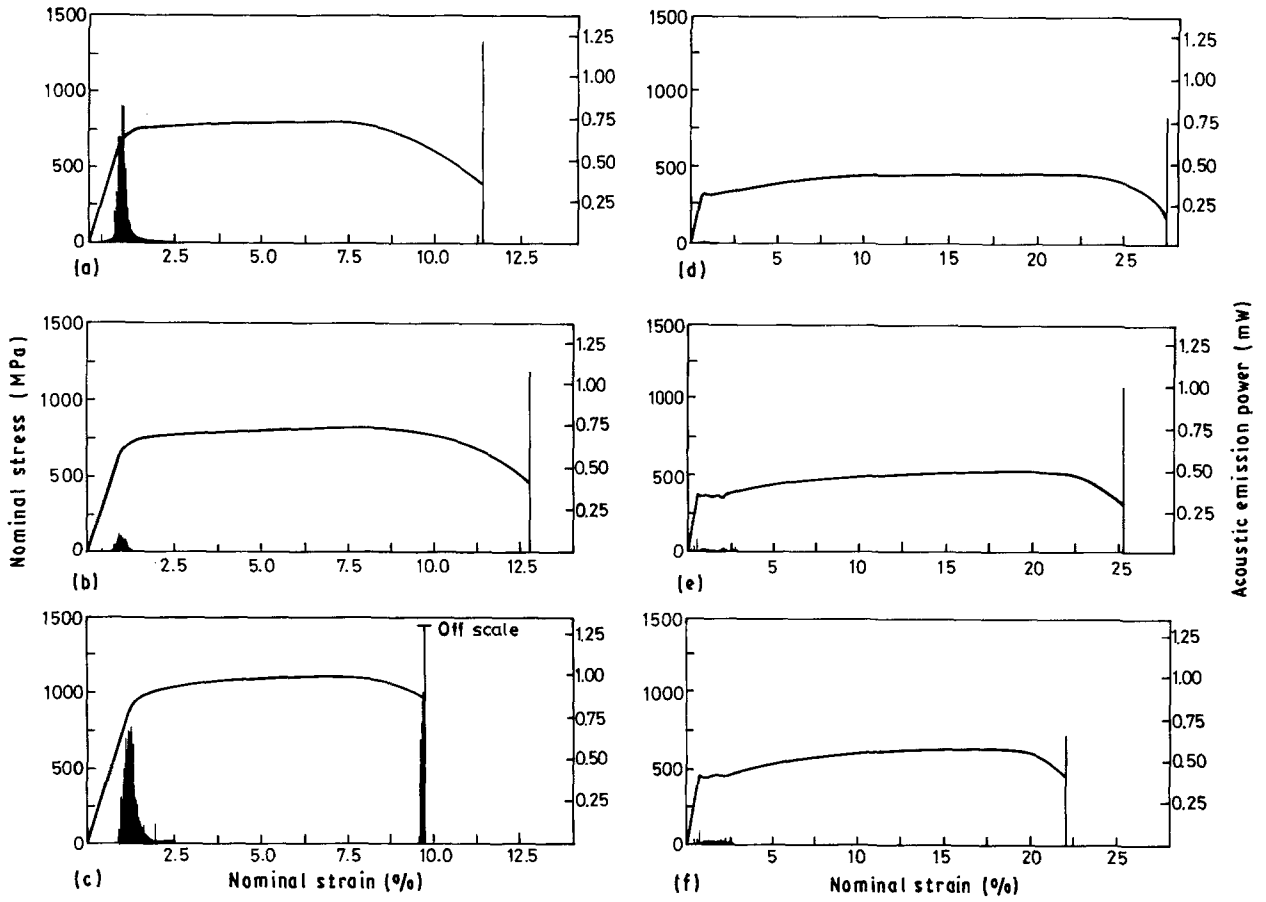

Figure 10 Acoustic emission and stress as functions of strain for specimens isothermally tempered at 625 °C (a–c) 10 min and (d–f) 40 000 min: (a, d) 0.06% C; (b, e) 0.17% C; (c, f) 0.49% C.

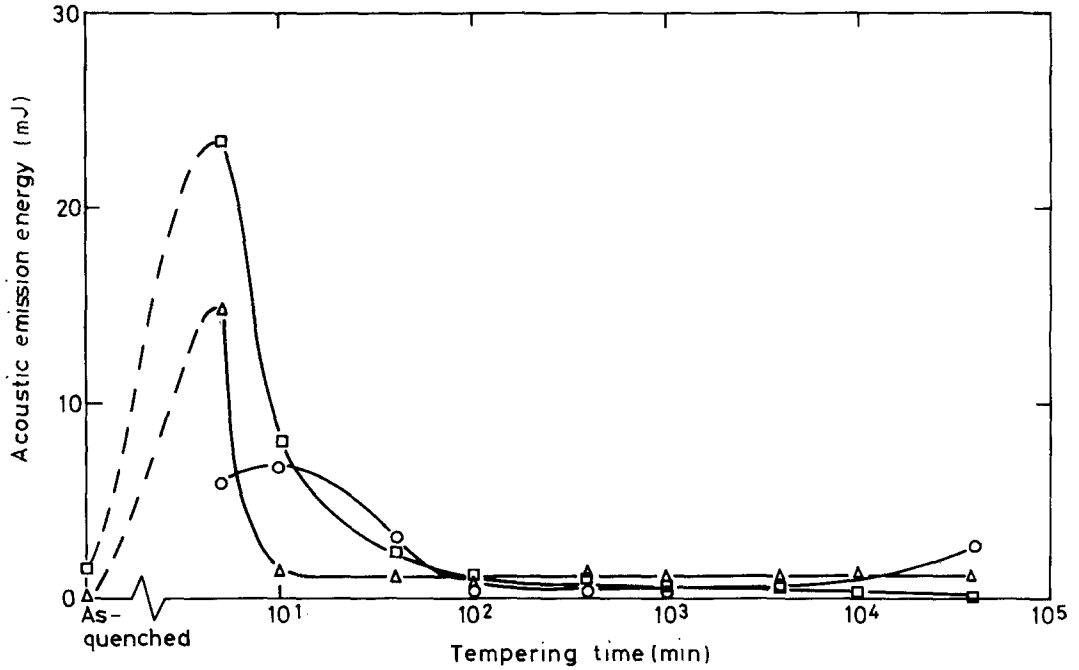

Figure 11 Effect of isothermal tempering at 625 °C upon acoustic emission from region I (deformation): (□) 0.06% C, (△) 0.17% C, (○) 0.49% C.

are probably an autotempering product, given the relatively high temperature at which the martensitic transformation begins. The martensitic start temperature (M_s) for alloy steels can be estimated from the relationship

$$M_s(°C) = 500 - 300C - 33Mn - 22Cr - 17Ni - 11Si - 11Mo$$

where C is the carbon content in wt %, etc. Thus, steels D, E and F have M_s temperatures of 383, 351, and

TABLE IV Mechanical properties for steels D, E and F as a function of isochronal tempering temperature

Treatment temperature (°C)	$\sigma_{0.1}$ (MPa)	$\sigma_{0.2}$ (MPa)	UTS (MPa)	Strain to σ_{UTS}	Ductility[a] (mm)	n-value	Work-hardening (rate) (GPa)
Steel D							
50	640	730	1035	0.032	2.85	0.09	–
95	615	720	951	0.036	2.93	0.15	19.4
143	770	828	1042	0.026	2.62	0.11	18.2
198	760	809	1030	0.027	2.48	0.10	16.0
250	745	805	980	0.019	2.47	0.11	17.2
283	760	800	1018	0.031	2.45	0.08	14.9
403	741	783	854	0.027	2.87	0.05	7.5
502	593	601	660	0.074	4.84	0.02	1.9
602	548	549	646	0.101	6.29	0.02	1.4
625	481	479	573	0.127	4.48	0.01	0.6
Steel E							
50	831	903	1292	0.045	2.40	0.11	25.0
95	849	910	1288	0.040	2.41	0.11	24.6
143	901	1003	1281	0.031	2.51	0.08	22.6
198	934	1036	1309	0.044	2.62	0.08	21.4
250	939	1030	1250	0.031	2.55	0.07	18.1
283	1001	1072	1277	0.036	2.44	0.06	16.8
403	945	1002	1112	0.041	2.84	0.04	8.6
502	690	701	791	0.075	4.74	0.03	3.7
602	634	638	742	0.083	4.48	0.04	2.1
625	589	593	701	0.104	5.67	0.03	1.3
Steel F							
50	1050	1233	1503	0.012	0.79	0.20	–
143	1246	1319	2397	0.052	1.55	0.26	42.4
198	1290	1400	2233	0.073	2.89	0.17	33.4
250	1370	1530	1931	0.046	2.13	0.08	25.9
283	1389	1445	1768	0.037	–	0.06	22.6
403	1202	1283	1426	0.029	1.80	0.04	15.3
502	834	856	1000	0.067	3.52	0.05	6.7
602	715	727	920	0.094	4.54	0.04	3.2
625	655	657	823	0.125	5.77	0.02	2.0

[a] 4 cm gauge length.

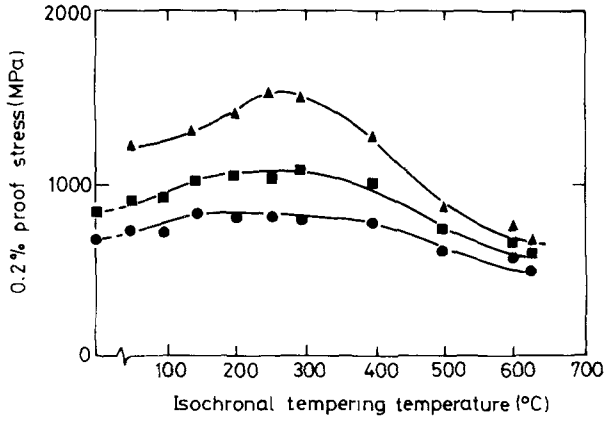

Figure 12 Effect of isochronal tempering upon 0.2% proof stress of Fe–3.25 wt% Ni alloys containing different carbon concentrations: (●) 0.06% C, (■) 0.17% C, (▲) 0.49% C.

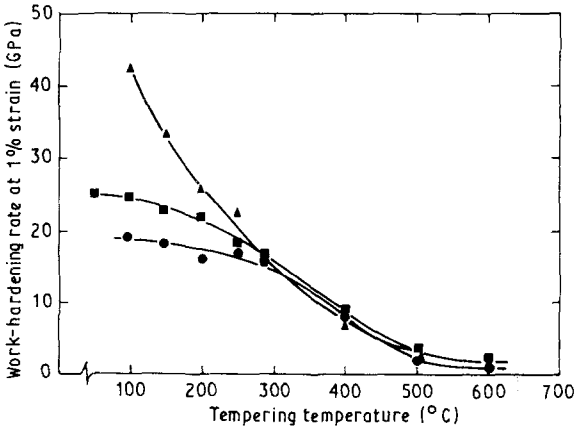

Figure 13 Effect of isochronal tempering temperature upon work-hardening rate at 1% plastic strain: (●) 0.06% C, (■) 0.17% C, (▲) 0.49% C.

263 °C, respectively. During oil quenching sufficient time exists for significant precipitation autotempering to occur in the low- and even the medium-carbon steels, but probably not in the high-carbon material.

Turning to the high-carbon material, Speich [9] has shown that a large fraction of the carbon which remains dissolved during quenching segregates to dislocations and internal interfaces, and only when the bulk carbon content exceeds about 0.2 wt % are these sites exhausted and interstitial supersaturation develops. Only steel F contained more than 0.2% carbon. In our earlier work [1] electron microscopy of this material indicated that rather than contributing to a supersaturated solution, some of the carbon formed very small coherent (possibly ε) carbides.

The effects of tempering these three steels can be summarized as follows:

TABLE V Mechanical properties for steels D, E and F as a function of isothermal tempering time

Treatment time (min)	$\sigma_{0.1}$ (MPa)	$\sigma_{0.2}$ (MPa)	UTS (MPa)	Strain to σ_{UTS}	Ductility[a] (mm)	*n*-value	Work-hardening rate (GPa)
Steel D							
5	909	927	1040	0.035	2.40	0.06	11.4
10	627	635	693	0.080	4.40	0.02	2.1
40	540	545	640	0.103	4.81	0.01	1.3
100	481	479	573	0.127	4.48	0.01	0.6
400	428	428	530	0.131	3.85	0.01	0.9
1000	413	406	523	0.146	4.03	0.01	0.7
4000	368	368	490	0.139	4.43	0.02	1.2
10000	338	340	471	0.152	4.31	0.02	0.9
40000	309	311	461	0.157	5.30	0.03	1.4
Steel E							
5	1020	1044	1268	0.021	2.26	0.09	16.6
10	703	716	821	0.079	5.01	0.03	3.8
40	637	645	752	0.088	5.63	0.02	2.2
100	589	593	701	0.104	5.67	0.03	1.3
400	548	548	667	0.103	5.91	0.01	1.2
1000	491	486	619	0.126	7.65	0.01	0.6
4000	427	430	583	0.126	4.08	0.02	1.9
10000	419	415	564	0.164	4.72	0.01	0.6
40000	350	349	506	0.186	4.79	0.01	0.4
Steel F							
5	1215	1294	1443	0.032	1.77	0.05	12.9
10	889	916	1089	0.072	3.41	0.05	10.7
40	696	709	863	0.096	5.57	0.02	3.4
100	655	657	823	0.125	5.77	0.02	2.0
400	586	590	752	0.130	7.17	0.02	0.8
1000	565	570	737	0.150	7.47	0.01	–
4000	510	504	689	0.148	4.93	0.01	0.9
10000	469	469	653	0.148	0.01	–	0.6
40000	363	367	535	0.181	4.04	0.01	0.3

[a] 4 cm gauge length.

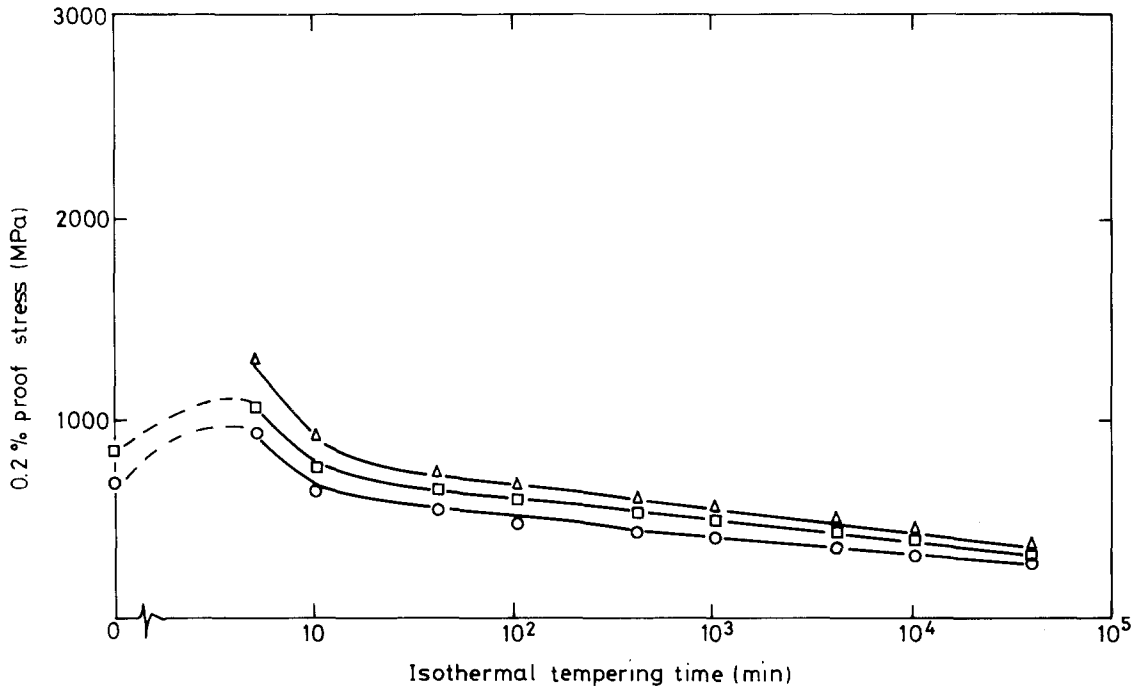

Figure 14 Effect of isothermal tempering upon the 0.2% proof stress: (○) 0.06% C, (□) 0.17% C, (△) 0.49% C.

(i) Below 200 °C the quenched-in carbides, dislocations and lath morphologies changed little. SANS and TEM observations indicated the precipitation of a high density of small (10–10 nm) carbides. Their size increased with tempering temperature.

(ii) Between 200 and 300 °C there was limited recovery of the quenched-in microstructure, while the temper-nucleated carbides increased in size.

(iii) Between 300 and 400 °C, the quenched-in microstructure underwent recovery, quenched-in car-

bides disappeared, lenticular-shaped carbides appeared at interfaces, and the average carbide size increased.

(iv) Above 400 °C, spheroidal carbides appeared and the quenched-in microstructure underwent recrystallization to an equiaxed polygonal ferrite.

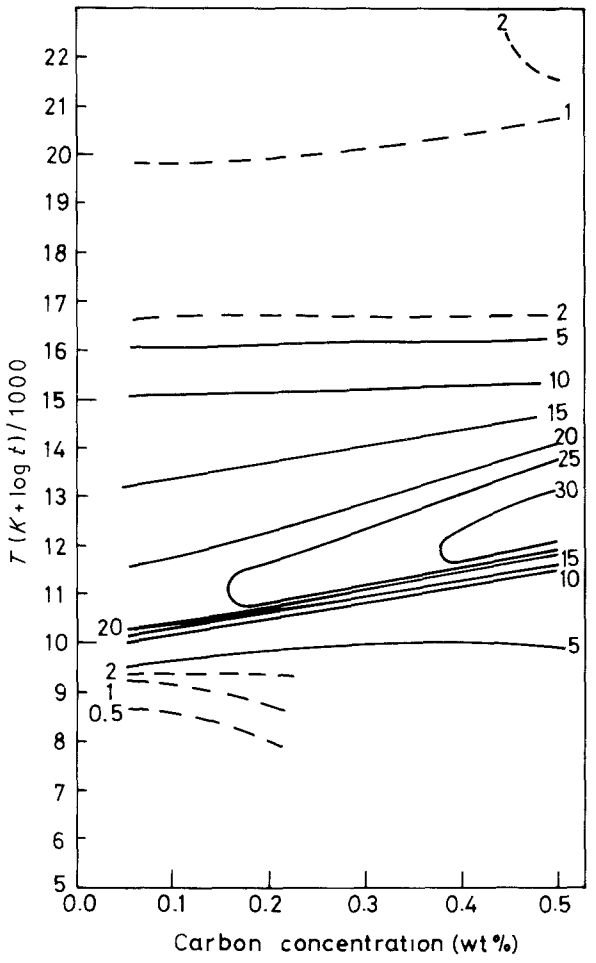

Figure 15 Map showing effect of tempering and carbon concentration upon the acoustic emission energy (mJ) detected during tensile deformation.

(v) Extended tempering at 625 °C increased the spheroidal carbide size, reduced the carbide spacing, and increased the ferrite grain size.

Because of the low emission from the quenched microstructures, it is reasonable to assume that their carbides do not act as direct emission sources. Furthermore, the decline in acoustic emission begins with the appearance of lenticular lath boundary precipitates, and suggests that these precipitates are not responsible for the low-temperature emission tempering peak. The origin of this effect therefore presumably lies in the interaction of dislocations with the fine precipitate distribution induced by light tempering.

4.2. Deformation mechanisms

In the steels used here, particularly for the treatments generating most emission, the mechanisms of deformation and their dependence upon microstructure are only superficially understood. Norstrom [10] and others have developed relationships between yield strength and microstructure for quenched and tempered steels. These are based upon Hall–Petch-like behaviour for dislocation–lath and dislocation–lath-packet boundary interactions. It is an implicit assumption that dislocations pile up at these internal interfaces (i.e. lath and lath-packet interfaces). There is some uncertainty about the ability of the lath boundaries within a given lath-packet to act as obstacles to dislocation motion. These are low-angle boundaries and some at least may allow dislocation propagation from lath to lath. However, the high-angle lath-packet interfaces are much less likely to allow such propagation, and probably are the primary microstructural feature controlling the distance of slip in precipitate-free material.

Precipitates both within and on the boundaries between laths and quenched-in dislocations provide additional impediments to dislocation motion. In

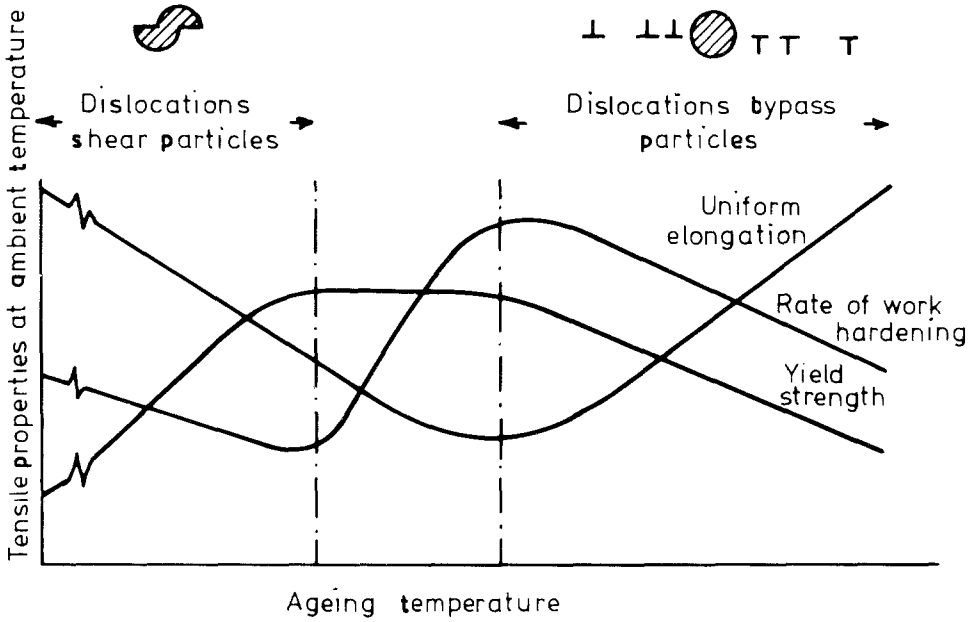

Figure 16 Schematic diagram of changes in tensile properties during ageing (after Hornbogen [12]).

quenched samples, which have heterogeneous precipitate distributions, those regions containing auto-tempered precipitates probably possess a considerably higher local yield stress, and deform later in a tensile test, after precipitation-free material has sufficiently work-hardened. These relatively large precipitates are unlikely to be sheared and slip probably requires an Orowan-like mechanism. In contrast, samples tempered below 300 °C contain numerous very small (possibly coherent) precipitates. In other alloy systems (e.g. age-hardened aluminium alloys) the precipitates in the underaged state are frequently too closely spaced for the (Orowan) bypass mechanism to be favoured, and precipitate shear occurs instead [11, 12]. This results in coarse slip bands (because a plane on which slip, and thus precipitate shear, has already occurred is less effectively hardened), low work-hardening rates, and decreased uniform elongations (Fig. 16) [12]. In aluminium alloys it has been found that slip in these microstructures is accompanied by intense levels of acoustic emission [4, 13, 14]. It is therefore interesting to speculate that such a precipitate shear process may also occur in the quenched and tempered microstructures that emitted such surprisingly intense emission.

The usual direct evidence of precipitate shear (from metallographic observations of slip patterns and electron micrographs showing shear bands) is inconclusive here because of the small separations between lath boundaries which make such observations impossible. Indirect evidence from mechanical property measurements provides support for a shearing process. First, the yield strength maximum, which normally characterizes the transition from shear to a bypass mechanism, is attained at about the same tempering temperature as the acoustic emission maximum. Second, the uniform elongation (strain to σ_{UTS}), which characterizes uniformity of slip, goes through a minimum close to the tempering temperature of maximum emission. Finally, a very pronounced decrease in work-hardening rate (at 1% strain) is observed as the tempering temperature increases. Much of this decrease is due to recovery of the quenched-in dislocation density, and indicates that forest interactions with the laths become greatly lessened after tempering above 250 °C, thus providing additional possibilities for slip concentration.

Tempering above 300 °C leads to the formation of larger, more widely spaced precipitates that can no longer be sheared, and correlates with a decline in emission. Particle size and interparticle spacing increase with tempering temperature and time, thereby lessening the contribution of precipitates to strengthening and promoting a more uniform slip distribution, and this correlates with the eventual loss of acoustic emission.

After very extended tempering treatments at 625 °C, samples begin again to generate emission and display yield points and Luders band deformation. All three effects are more pronounced in the high-carbon samples. Tempering of those recrystallized microstructures leads to an increase in grain size and intercarbide spacing and thus dislocation mean free path before pinning. After cooling from 625 °C, interstitial locking of dislocations is probable, and yield is characterized by the generation of fresh dislocations that do not have interstitials at their cores. One expects the velocity of these fresh dislocations to be related to the applied stress by a Johnson and Gilman type equation:

$$v = \left(\frac{\sigma}{\sigma_0}\right)^m$$

where σ is the yield stress, σ_0 a reference stress, and m a material index (> 1). Since the yield stress increases with carbon concentration, we might expect a greater dislocation velocity during unstable slip in the higher-carbon alloys.

4.3. Acoustic emission micromechanisms

There are two separate mechanisms of dislocation motion that can apparently generate acoustic emission in these alloys. One is the motion of dislocations through a martensitic microstructure containing small, closely spaced precipitates; the second is the unstable movement of dislocations through ferrite subgrains essentially devoid of interior precipitates.

Consider first a hypothetical slip process in an idealized martensitic microstructure (Fig. 17a). A series of dislocation loops is emitted by a dislocation source, each of which expands rapidly until arrested. Dislocations whose glide plane is coplanar with the lath habit plane are arrested by the lath-packet boundary. Dislocations at some other angle to the habit plane may interact with lath boundaries, which are low-angle and may provide a relatively weak slip barrier. Thus, irrespective of glide plane–habit plane angle, it is quite likely that the maximum dislocation glide distance is the lath-packet size, typically 10 μm here.

Then, for the process depicted in Fig. 17a we can compute the total area swept out by the loops (170 μm^2) and the duration of the event, assuming each loop had a radial velocity close to the speed of sound, say 2000 $m\,s^{-1}$ (Fig. 17b). For simplicity, we can equate this process to a single dislocation loop of 7.5 μm radius, expanding to cover the same area (170 μm^2) in the same time, (Fig. 17c). Its average radial speed v would be ~ 1000 $m\,s^{-1}$. Then we can use the acoustic emission detectability criterion, $av \geq 0.03$ $m^2\,s^{-1}$ (a is slip distance, v is slip speed) to determine if such an event is detectable [1, 15]. The product av for a single 7.5 μm loop expanding at 1000 $m\,s^{-1}$ is in fact 0.0075 $m^2\,s^{-1}$, i.e. too small to be detected.

For the process depicted, about 40 dislocations moving in synchronism (so that their signals are in phase and their amplitudes add) are required to give a detectable signal. Such cooperative motion requires the existence of a mechanism to coordinate the slip. The shear of precipitates and resultant slip localization is one such process. If we imagine the precipitates to be successively sheared by dislocations, we see that as they are sheared they are progressively weakened, and provide lessened glide plane resistance (Fig. 18).

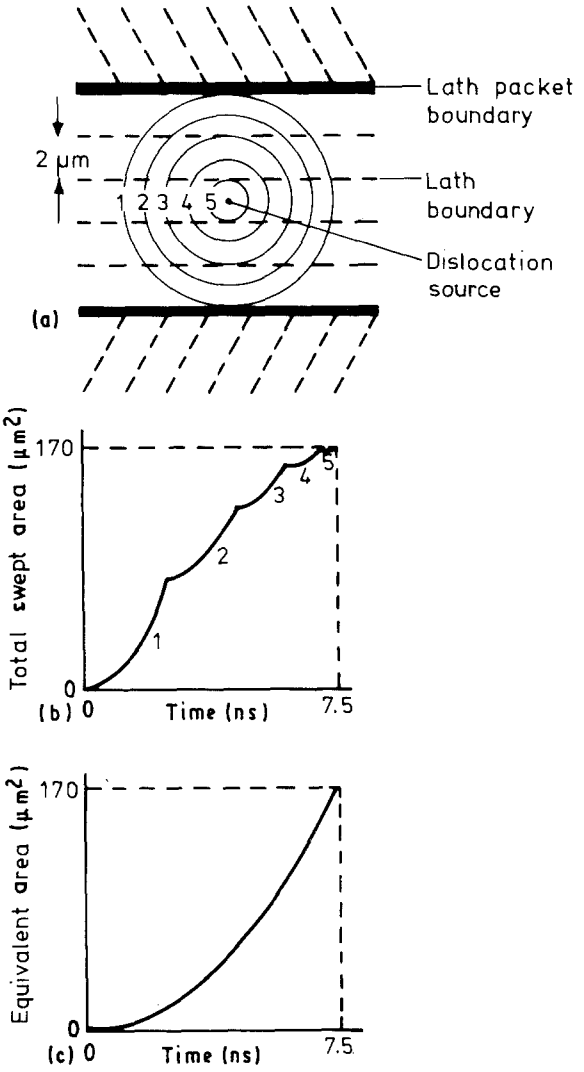

Figure 17 Series of dislocation loops emitted by single source are eventually arrested at lath-packet boundary. Area swept out by loops controls acoustic emission amplitude. For simplicity, a single loop of equivalent area is used to estimate source detectability.

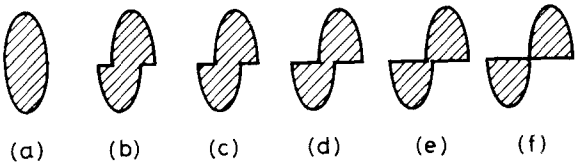

Figure 18 A small precipitate offers less resistance to successive dislocations (a–f) as it undergoes shear.

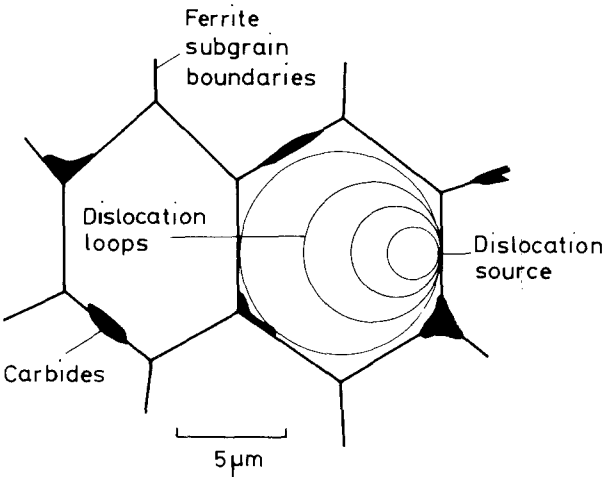

Figure 19 Schematic diagram showing four dislocation loops expanding radially from source on grain boundary.

This creates a glide plane into which deformation localizes until the forward stress on the dislocation is balanced by the back-stresses from dislocations piled up at the lath-packet boundaries. This process appears most consistent with our acoustic emission observations.

Such a process accounts both for the rather weak (cf. tempering) effect of carbon concentration upon the intense emission of lightly tempered microstructures and for the lack of emission from the as-quenched state. In the latter case no small precipitates are present to concentrate slip. The former effect is observed because the size of precipitates is the most important factor; the volume fraction is of secondary importance.

The second micromechanism of acoustic emission in extensively tempered samples seems not to be connected with dislocation–precipitate interactions, but rather with the rapid multiplication of dislocations during a microyield event. In Fig. 1 we schematically depict a "slip event" during the initial (Luders) deformation of a fully recovered microstructure. The distance the dislocations move before arrest is controlled by the subgrain size (~ 5 μm typically). A single dislocation nucleated at a grain boundary would have to move at a supersonic velocity to generate an emission exceeding the detection threshold $av \geq 0.03\ m^2\ s^{-1}$. Four or five dislocations moving in synchronism at the more physically realistic velocity of $1000\ m\ s^{-1}$ (30% shear-wave speed) would be just detectable. Such events have a higher probability of occurrence when the initial dislocations are locked by an atmosphere of interstitials. Then, only a few sources are active at any one time, and the imposed strain rate is satisfied by high-velocity dislocation motion increasing the probability of accompanying detectable acoustic emission.

Finally, we note that Jaffrey [16], after a lengthy review of acoustic emission source mechanisms, concluded that the importance of carbide fracture as a source of acoustic emission remained undecided. Numerous sizes and shape distributions of carbides have been tested in this and the earlier study [1]. In no case has a clear role for carbide fracture itself as an emission source been identified, and we must therefore conclude that only in very special cases (e.g. grain-boundary cementite films or very coarse pearlites) may the carbide fracture process itself be considered a detectable emission source.

5. Conclusions

The generation of detectable acoustic emission in three quenched low-alloy steels has been found to be highly sensitive to tempering. In particular:

1. An isochronal tempering peak in acoustic emission activity, located at a tempering temperature of $\sim 300\,°C$, has been identified in all three steels. It is

only weakly affected by carbon content and coincides with the tempering temperature that gives maximum yield stress. TEM and SANS studies indicate that the peak correlates with the presence of a dense dispersion of very small precipitates.

2. The origin of the tempering emission peak is proposed to be the motion of groups of dislocations over distances of about the lath-packet dimension. Single dislocations are shown to be incapable of generating detectable acoustic emission by this process. The concentration of slip, by for example precipitate shear, is able to account for the emission observed.

3. A weaker acoustic activity has been observed in material subjected to prolonged tempering at 625 °C. This emission is more strongly affected by carbon concentration. It originates from the collective motion of groups of dislocations over distances comparable with the subgrain size. Such collective motion arises because of the initially very low mobile dislocation density. The increased emission of high-carbon (high yield stress) samples is attributed to a strong effect of upper yield stress upon dislocation velocity.

4. No evidence has been found in this work to support the proposition that in quenched and tempered steels carbide fracture is a direct source of detectable acoustic emission.

Acknowledgements

We are indebted to Drs B. Pickering, B. L. Eyre and J. A. Hudson for helpful discussions of this work. We are grateful to P. Lane, A. Bartlett and C. Glinka for assistance with various aspects of the experimental work. This research was principally funded by the Ministry of Defence (Procurement Executive) through the Admiralty Research Establishment, Holton Heath, Dorset, UK.

References

1. H. N. G. WADLEY and C. B. SCRUBY, *J. Mater. Sci.* **26** (1991) 5777.
2. H. N. G. WADLEY, C. B. SCRUBY, P. LANE, and J. A. HUDSON, *Met. Sci.* **15** (1981) 514.
3. J. F. KNOTT, Private Communication.
4. H. N. G. WADLEY, K. RUSBRIDGE and C. B. SCRUBY, *Mater. Sci. Eng.* **59** (1983) 169.
5. J. R. WEERTMAN, in "Nondestructive Evaluation: Microstructural Characterization and Reliability Strategies", edited by O. Buch and S. Wolf (TMS-AIME, Pittsburgh, Pa, 1980) 147.
6. V. GERALD, *J. Appl. Crystallogr.* **11** (1978) 376.
7. H. N. G. WADLEY and C. B. SCRUBY, *J. Mater. Sci.* **28** (1993) 2517.
8. C. B. SCRUBY and H. N. G. WADLEY, *ibid.* in press.
9. G. R. SPEICH, *Trans. Met. Soc. AIME*, **245** (1969) 553.
10. L. A. NORSTROM, *Scan. J. Metall.* **5** (1976) 159.
11. E. HORNBOGEN and K. GAHR, *Metallography* **8** (1975) 181.
12. E. HORNBOGEN, *Trans. ASM* **57** (1964) 121.
13. H. N. G. WADLEY and C. B. SCRUBY, *J. Mater. Sci.* **12** (1978) 285.
14. K. L. RUSBRIDGE, C. B. SCRUBY and H. N. G. WADLEY, *Mater. Sci. Eng.* **59** (1983) 151.
15. C. B. SCRUBY, C. JONES, J. M. TITCHMARSH and H. N. G. WADLEY, *Met. Sci.* (1981) 241.
16. D. JAFFREY, *Aust. Chem. Eng.* (Nov/Dec 1979) 9.

Received 21 July
and accepted 2 September 1992